SIMULATION STUDIES FOR SURFACES AND MATERIALS STRENGTH

Semiannual Progress Report

for
Cooperative Agreement NCC2-297

for the period
May 1, 1991 - October 31, 1991

Submitted to

National Aeronautics and Space Administration
Ames Research Center
Moffett Field, CA 94035

Computational Chemistry Branch
Dr. Steve Langhoff, Chief

Thermosciences Division
Dr. Jim Arnold, Chief

Prepared by
Eloret Institute
1178 Maraschino Drive
Sunnyvale, CA 94087
Phone: 408 730-8422 and 415 493-4710
K. Heinemann, President and Grant Administrator
Timur Halicioglu, Principal Investigator

During this period investigations were carried out in three areas:

1. A simulation study was conducted to investigate very early stages of a nucleation and growth mechanism taking place on diamond surfaces. The energetically most favorable binding sites were calculated along with the binding energies for up to three carbon adatoms deposited on (100) and (111) planes of a diamond crystal. Bindings for carbon atoms deposited on the (100) plane were found to be much stronger than the (111) case. Based on purely energetic considerations, results obtained in this investigation indicate that the nucleation of carbon atoms should take place more favorably on the (100) plane than on the (111) plane. Calculated high energy sites for adatoms on the (100) plane were found to be commensurate with atomic sites within the surface region of the crystal. Computational details along with a short discussion of the results are presented in Appendix 1.

2. Calculations were carried out in this investigation to analyze energies and structural properties for (2×1) restructured patterns of the (100) surface of diamond. Two different model functions developed recently for carbon were employed in calculations. Three differently reconstructed (2×1) patterns (namely, one dimer model and two different missing row models) for the exposed surface layer, were taken into consideration. Results obtained in this investigation support the stability of the dimer model over the unreconstructed (1×1) surface. Calculated energies and structural properties for the dimer model were found to be in agreement with values obtained in other theoretical calculations. While one of the potential functions, in accordance with common belief, predicted the dimer model for the (2×1) restructured surface to be the energetically most stable structure, the other function produced one of the missing row models as the most favorable form. Appendix 2 includes details of the calculated results and a discussion on the configurational aspects

of (2×1) restructured surfaces.

3. In this part, a crack propagation process for the graphitic basal plane, was investigated using a molecular dynamics technique. Interactions among carbon atoms in the system were calculated using the Tersoff potential energy function. This function is based on two- and three-body interactions and produces many macroscopic properties of carbon species correctly. In addition to individual atomic energies, stress tensors for every atom in the system, were also calculated. Simulations were performed for a system containing up to 1600 carbon atoms and bearing an initial crack. After an equilibration period the system was loaded uniaxially in a direction perpendicular to the existing crack with small incremental elongations. Further equilibrations caused the crack to propagate. During this crack propagation process, atoms located at the tip of the crack were found to have very high stress values. This result is in general agreement with other reported calculations and with existing theories based on macroscopic considerations. However, no dislocation formation in front of the advancing crack was found. This outcome was attributed to the short range nature of the potential function employed in this study. Results are presented in Appendix 3.

Appendix 1. Modeling for Early Stages of Diamond Growth

An atomic level understanding of the very early stages of a nucleation process is highly desired today in different disciplines related to crystal growth [1-3]. In this study a simulation calculation was performed to investigate early stages of the diamond growth mechanism. Binding energies and binding sites were determined for a number of carbon atoms deposited on (100) and (111) faces of a diamond crystal. Calculations were carried out for the low temperature limit and throughout this investigation model potential functions developed recently for carbon species were used. For comparison, two different model functions, based on two and three-body interactions, were considered here. The first potential is the Tersoff function. It has been shown that this function is able to reproduce correctly various bulk properties of diamond and of the graphitic plane [4]. The second potential used in this study is the Brenner function [5] which is analytically similar to the Tersoff function, but parametrized differently. This function also, has been shown to produce acceptable results for properties of bulk diamond and the basal plane of graphite, as well as for some properties of small carbon clusters [5,6].

Binding energies per adatoms, E_b, were calculated as:

$$E_b = \frac{1}{m}[E_s^{(m)} - E_s^o]$$

where m is the number of adatoms, E_s^o denotes the total equilibrated energy of the system of N particles with an exposed surface, and $E_s^{(m)}$ is the total relaxed energy of the same system with m adatoms deposited on the surface. In this investigation (100) and (111) index planes of a diamond crystal were taken into consideration. Surfaces were first generated as abrupt terminations of bulk diamond oriented to produce the desired surface planes. Systems bearing these faces were then relaxed

using a molecular dynamics procedure. Periodic boundary conditions in two directions (parallel to the exposed surface) were imposed on the system to provide the continuity of the surfaces. At low temperature these planes remain in (1×1) patterns after the relaxation, but results indicate that for both surface planes the top interlayer spacings contract considerably, while the second interlayer spacings exhibit a moderate expansion [7]. Next, carbon atoms were positioned on these fully relaxed surfaces in various configurations and the whole system (now including adatoms) was reequilibrated with the same procedure. Up to three adatoms were deposited on these surface planes and for each case a number of binding sites were considered in calculations. Only the energetically most favorable sites are reported here.

A top view of the (100) surface plane of diamond is depicted in Figure 1 which shows lattice sites for atoms located in the top four layers. Calculations using both Tersoff and Brenner functions produced an upper bridge site (which is the mid-point between two neighboring upper layer atoms) as the energetically most favorable site for a single adatom. One of these sites is denoted by the letter A in Figure 1. These upper bridge sites are located exactly above the atoms in the fouth layer and they represent exact positions for adatoms forming a complete monolayer coverage over the (100) plane of diamond. Calculated values for binding energies are given in Table 1. Equilibrated positions for the adatom in this case, were found to be about 0.9 and 0.85 Å above the surface plane for the Tersoff and Brenner functions, respectively. For two adatoms deposited on the (100) plane the lowest energy configuration using the Tersoff function was found to be the two neighboring upper bridge sites denoted by A and D in Figure 1. For the Brenner function, on the other hand, the two opposing upper bridge sites indicated by A and B are more favorable. In this case also, after the equilibration, adatoms were found to be located approximately 0.9 and 0.85 Å above the surface plane for the Tersoff and and Brenner functions, respectively. In the case of three adatoms, both functions

produce sites A, B and C (see Figure 1) as the energetically most favorable sites. The adatom at site C in this case is located about 1.75 Å above the surface plane for the Tersoff function and about 1.65 Å above the surface for the Brenner potential. In both cases, the deposited trimer in its fully relaxed configuration forms an obtuse isosceles triangle with an apex angle of approximately 113 degrees.

In the case of the (111) plane, lattice sites for atoms located in the top four layers are shown in Figure 2. For an unrelaxed surface, only one type of interplanar spacing exists for the (100) plane. For the (111) plane, however, atomic layers come in pairs and form two different types of interlayer spacings. For an ideal case, the first interlayer spacing, δ_{12} is just $\frac{1}{3}$ of the second interlayer spacing, δ_{23}, which is equal to the nearest neighbor distance in the crystal. In (111) plane, a considerable amount of shrinkage takes place in δ_{12} upon relaxation [7]. Calculations using both the Tersoff and Brenner functions, produced the energetically most favorable site for a single adatom on the (111) surface plane at a top position. The location for one of these binding sites is denoted by the letter A in Figure 2. The optimized position of an adatom was calculated as 1.49 and 1.38 Å exactly above the surface atom for the Tersoff and Brenner functions, respectively. In both cases, calculated results also indicate that the surface atom at site A moved upward for a few tenths of an angstrom above the surface plane. For a dimer deposited on a relaxed (111) surface, calculations based on Tersoff function produced adatom positions near two neighboring top surface atoms as the energetically most favorable sites (A and B as shown in Figure 2). In its fully relaxed configuration adatoms of the deposited dimer are about 1.62 Å above the top layer. Adatoms in this case are not exactly above the sites A and B but displaced symmetrically toward each other. Equilibrated adatoms were found to be aligned parallel to the AB line with an interatomic distance of 1.48 Å. In this case also, surface atoms at sites A and B relaxed upwards for approximately two tenths of an angstrom. For the Brenner function the relaxed configuration of a dimer is somewhat different. In this case, adatoms were found to be aligned above the line connecting the sites A and C. One of the adatoms was

located between A and D about 1.67 Å above the surface plane while the other adatom was found to be between C and D about 1.92 Å above the surface. In this fully equilibrated configuration the distance between two adatoms was calculated as 1.36 Å. Surface atoms at sites A and C were found to be relaxed upwards about 0.3 and 0.6 Å above the surface plane, respectively. In this case it is worthwhile to indicate that the atom at site C was located in the second layer before the relaxation. In the case of three adatoms, both functions produced comparable results. Adatoms, in their energetically most stable configuration, are located near the sites A, D and C (see Figure 2). For the Tersoff function adatom positions were found to be about 1.73, 2.53 and 1.99 Å above the surface plane, while the Brenner function produced 1.71, 2.43 and 1.98 Å, respectively. In both cases, adatoms form an obtuse isosceles triangle with an apex angle of approximately 125 degrees and bond distances were calculated as 1.46 and 1.31 Å for the Tersoff and Brenner functions, respectively. After relaxation, in this case also, surface atoms at sites A and C were found to be displaced upward approximately 0.2 and 0.5 Å for the Tersoff function and about 0.3 and 0.6 Å for the Brenner function.

Calculated results for E_b reported in Table 1 indicate that binding of adatoms on the (100) surface is energetically more favorable than binding on the (111) plane. At least up to $m = 3$, high energy adsorption sites on the (100) face were found to be commensurate with the atomic sites on the surface of the crystal. However, high energy positions for adatoms (of dimers and trimers, in particular) deposited on the (111) plane, are only partially commensurate with the lattice sites. Both potential functions produced comparable results. Closer analysis of structures of equilibrated trimers, reveals that at its very early stages a nucleus formed on the (100) plane is more likely to have a diamond character than one forming on the (111) surface. Based on purely energetics considerations, results obtained in this study indicate that carbon atoms nucleate on the (100) surface more readily than on the (111) plane. In comparing these results with experimental findings, however,

extreme care should be exercized. Calculations carried out here employing model functions reflect energetics of the nucleation process for systems containing only carbon atoms. No consideration was given in this investigation to the entropic or kinetic aspects.

References

[1] V. Bortolani, N. H. March and M. P. Tosi (eds), *Interaction of Atoms and Molecules with Solid Surfaces*, Plenum Press, New York, 1990.

[2] R. Hull, J. M. Gibson and D. A. Smith (eds), *Initial Stages of Epitaxial Growth*, Materials Res. Soc. Symp. Proc., Vol. 94, 1987.

[3] W. A. Tiller, *The Science of Crystallization: Microscopic Interfacial Phenomena*, Cambridge Univ. Press, 1991.

[4] J. Tersoff, Phys. Rev. Lett., **61**, 2879 (1988).

[5] D. W. Brenner, Mater. Res. Soc. Symp. Proc., **141**, 59 (1989).

[6] T. Halicioglu, Chem. Phys. Lett., **179**, 159 (1991).

[7] T. Halicioglu, Surface Sci. (in print, 1991).

Table 1. Calculated binding energies for carbon atoms deposited on (100) and (111) planes of diamond.

Surface Plane	Number of Adatoms	Tersoff E_b (eV)	Brenner E_b (eV)
(100)	1	-7.4715	-7.8397
	2	-7.5162	-7.8413
	3	-7.6803	-7.9653
(111)	1	-3.5956	-3.5210
	2	-4.8372	-5.4031
	3	-5.7485	-5.9351

Figure 1. A top view for the (100) surface plane of diamond. Atomic sites in the top four layers (parallel to the exposed surface) are shown. Open large and open small circles represent atomic sites in the first and second layers, respectively. Solid large and solid small circles are atomic sites in the third and fourth layers.

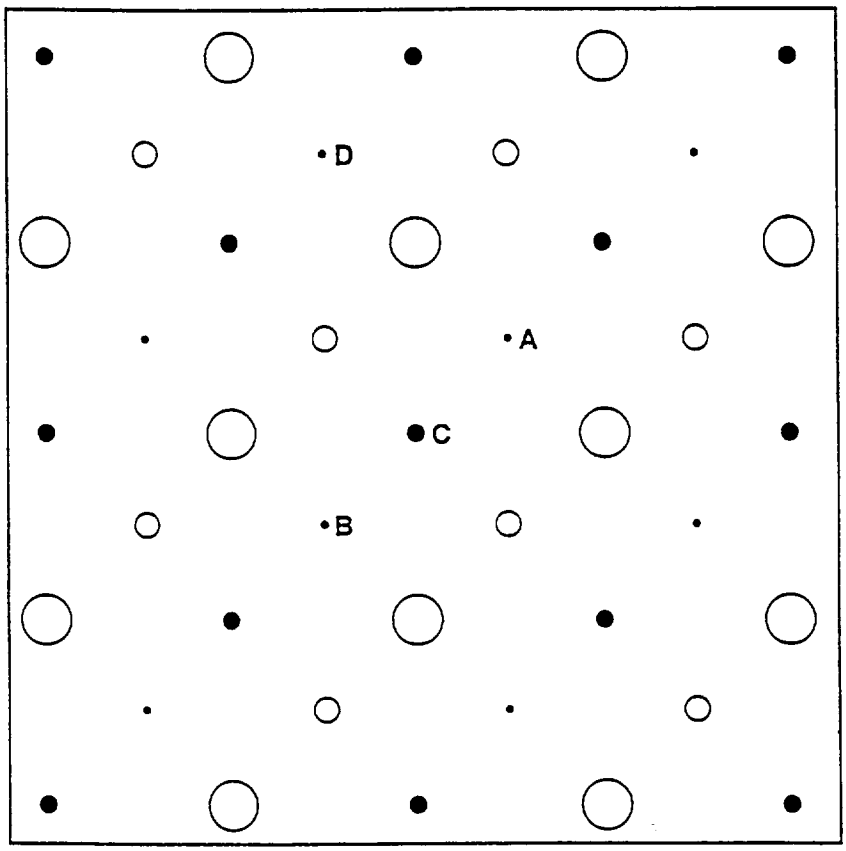

Figure 2. A top view for the (111) surface plane of diamond. Atomic sites in the top four layers (parallel to the exposed surface) are shown. Open large and open small circles represent atomic sites in the first and second layers, respectively. Solid large and solid small circles are atomic sites in the third and fourth layers. In this case, atoms located in the second and third layers are superimposed.

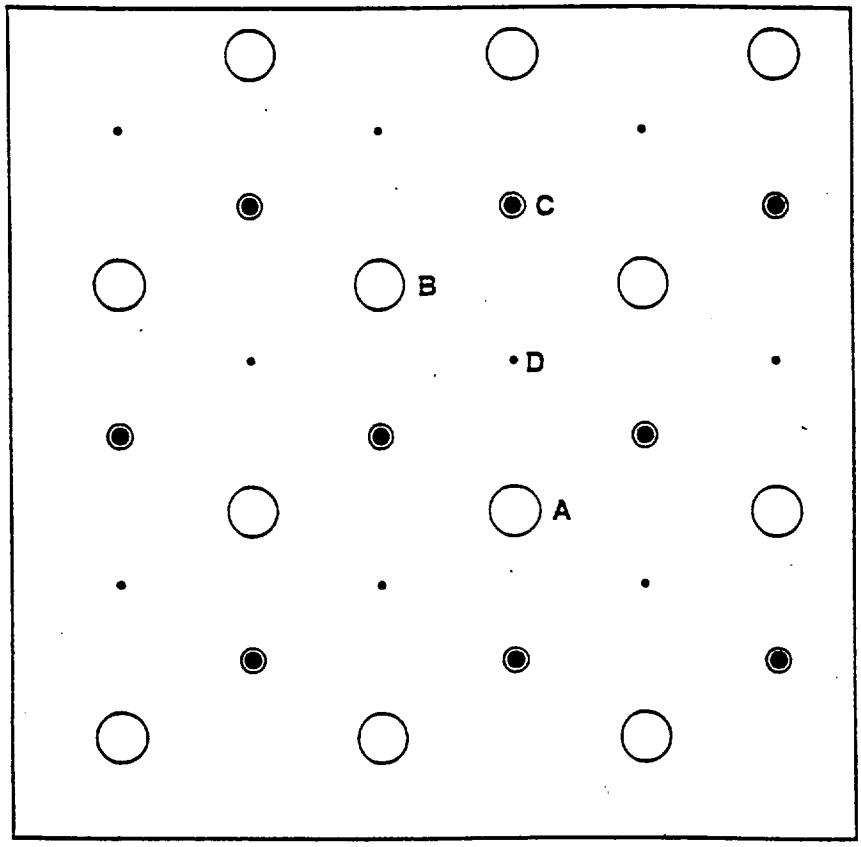

Appendix 2. (2×1) Reconstructed Patterns of Diamond (100) Surface

Simulation calculations were performed to investigate (2×1) reconstructed patterns for the (100) surface of diamond. Model potential functions developed recently for carbon species were used throughout this study. For a better analysis, two different model functions, based on two and three-body interactions, were considered here. The first potential is the Tersoff function [1]. It has been shown that this function is able to reproduce correctly various bulk properties of diamond and of the graphitic plane. The second potential used in this study is the Brenner function [2] which is analytically similar to the Tersoff function, but parametrized differently. This function also, has been shown to produce acceptable results for properties of bulk diamond and the basal plane of graphite, as well as for some properties of small carbon clusters [2,7]. While the Tersoff function reproduces correctly the lattice constant of diamond, the Brenner potential at its minimum energy configuration gives a lattice constant value about 3% shorter.

Relaxed and unrelaxed surface energies for low index planes of diamond for unreconstructed (1×1) patterns have recently been calculated using Tersoff and Brenner functions [8]. Unrelaxed surfaces created as abrupt terminations of the bulk have been found to undergo a multilayer relaxation process upon equilibration. While a freshly created diamond (100) surface exhibits no LEED patterns, after heating to about 500 K in high vacuum it displays (1×1) patterns [3]. This surface, however, exhibits (2×1) patterns upon further heating to above 1300 K. Experimental evidence indicates that in this restructuring process the role of hydrogen is significant. At the present time, it is generally believed that at high T, most of H is desorbed from the surface region, and the observed (2×1) LEED patterns are due to the formation of dimer pairs by analogy with the Si and Ge (100) surfaces. There are several theoretical calculations supporting the dimer formation model for the clean (100) surface of diamond. Recently, Mehandru and Anderson

[4] calculated the energy change associated with the dimerization process based on a six-layer-thick slab model. In their calculations they employed a tight binding method (ASED-band) and demostrated that dimer formation is energetically favorable. Similarly, Bechstedt and Reichardt [5] using an energy minimization procedure based on a self-consistent tight-binding method, have concluded that a (2×1) reconstructed (100) surface of diamond is energetically more stable than the unreconstructed (1×1) structure. Furthermore, considering a C_9H_{12} cluster (as a representative of the (100) surface) Verwoerd [6] has employed a MNDO procedure to calculate the minimum energy configuration of the top layer. His results also indicate that the dimer formation process is energetically favorable.

In this investigation to determine relaxation energies as well as other structural properties for differently restructured (2×1) patterns of the (100) surface of diamond, we carried out energy minimization calculations using both Tersoff and Brenner functions. A typical computational cell consisted of a 16-layer slab containing about 256 atoms. Periodic boundary conditions were imposed on the system in two directions (i.e., x and y) and the third direction, z, was left free to provide exposed surfaces. Computational cell sizes in these calculations were chosen to satisfy minimum energy conditions for corresponding potential functions [1,2]. The relaxation energy, ΔE, was calculated as the difference in energies between a completly equilibrated system with a (2×1) structured surface and a system with an unrelaxed (1×1) face. Accordingly, the value of ΔE reflects the gain in stability as a result of restructuring and relaxation.

The (100) surface of diamond with different (2×1) reconstruction patterns was taken into consideration. In addition to the (2×1) dimerized pattern, two different types of missing row models were also included in the calculations. In the first missing row (MR) structure, the top layer atoms located in every other row were removed from the system. A top view of the (MR) structure is shown in Figure 2,

while Figure 1 depicts the unreconstructed (1×1) surface. The (MR) structure was obtained by removing alternating row atoms from an ideal (100) surface. (This surface structure is not identical with the structure obtained by removing alternating column atoms.) In this study, only the missing row model as shown in Figure 2 was investigated. In the second missing row model, those atoms removed to generate the (MR) structure, were placed on bridge sites along the rows formed by the remaining top layer atoms. Those displaced atoms now form a new layer which will be called the 0'th layer. This model will be referred to as (MR+1) and its top view is depicted in Figure 3. A schematic top view of the (2×1) restructured dimer model is shown in Figure 4. This picture depicts dimers formed between the atoms within the same row. The other (2×1) dimer model which may be formed by pairing the column atoms, was found to be energetically less favorable. Therefore, in this investigation only the row-dimer model, as shown in Figure 4, was taken into consideration.

For the (2×1) dimer model, calculated relaxation energies along with the structural parameters are compared in Table 1 with other available data from the literature. While the gain in energy during the relaxation process calculated by the Tersoff function is smaller than the values of Mehandru and Anderson [4] and of Verwoerd [6], it is consistent with the value reported by Bechstedt and Reichardt [5]. On the other hand, the Brenner function produced a more negative ΔE value which shows, in a way, a better general agreement with reported values. The distance between two carbon atoms in a dimer, r_{dimer}, calculated using the Tersoff function is in very good agreement with the value reported by Bechstedt and Reichardt [5]. On the other hand, the value of r_{dimer} obtained by the Brenner function is consistent with the reported value of Verwoerd [6]. Relatively speaking, both functions produced dimer distances in fair agreement with the literature values listed in Table 1. In addition, both the Tersoff and Brenner functions predict symmetric dimers that agree with findings of Verwoerd [6] as well as with results of Mehandru and Anderson [4].

Multilayer relaxation features for the (2×1) dimerized (100) surface calculated by the Tersoff and Brenner functions are qualitatively consistent with each other. SimilarOB to the (1×1) unstructured case reported earlier [8] for the dimerized (2×1) case also, interlayer spacings in the surface region exhibit alternating contractions and expansions with decreasing magnitudes as departing from the exposed surface. In this respect, results obtained here using the Tersoff as well as the Brenner functions are in general agreement with values of Mehandru and Anderson [4]. See Table 1. The change due to the relaxation in the interlayer spacing between the i and j planes is denoted by Δh_{ij} and the corresponding percentage change with respect to the unrelaxed system is δ_{ij}. The largest relaxation takes place in the first interlayer spacing which is the separation between the first and second surface planes parallel to the exposed surface. The value of Δh_{12} obtained using the Tersoff function lies between the values reported by Mehandru and Anderson [4] and Verwoerd [6]. The Brenner function, on the other hand, produces a slightly larger value for Δh_{12}, but it is still in good agreement with the value of Verwoerd [6]. (See Table 1). Calculated values for Δh_{23} and Δh_{34} are very small. The Tersoff function predicts almost no relaxation for interlayer spacings between the third and fourth layers. When compared with reported values of Mehandru and Anderson [4], the Tersoff function, in general, predicts sligthly smaller values, while the Brenner function produces somewhat larger relaxation for the interlayer spacings.

Calculated results obtained by the Tersoff and Brenner functions for the missing row models, (MR) and (MR+1), are presented in Table 2. Tabulated values for ΔE indicate that for these missing row models the Brenner function provides more relaxations than the Tersoff potential. The same trend is also true for the dimer model. When those values are compared with relaxation energies given in Table 1, the energetically least stable (2×1) restructured surface (for both functions) was found to be the (MR) model. The Brenner function predicts the dimer model to be the most favorable structure (among those three models considered in this investigation). It is about 0.18 eV per surface atom more stable than the (MR+1)

model. The Tersoff potential, on the other hand, predicts the (MR+1) structure to be the energetically most stable one. It was found to be 0.325 eV per surface atom more stable than the dimer model. Upon equilibration these missing row models also exhibit strong multilayer relaxation features. (See Table 2). For the (MR+1) model the relaxation patterns are qualitatively similar to the dimer model case with alternating contractions and expansions. For the (MR) model, however, the multilayer relaxation features are somewhat different. In this case, both first and second interlayer spacings shrink during the relaxation while the third interlayer spacing displays a relatively small amount of expansion. In addition to changes in interlayer spacings, relaxation in the case of these missing row models, also produces small lateral motions for some atoms. Those atoms located in the second layer were found to be displaced (with respect to their lattice positions) in a direction perpedicularly away from the missing row location. See Figures 2 and 3. For the (MR) case displacements were calculated as 0.07 and 0.11 Å corresponding to the Tersoff and the Brenner functions; and for the (MR+1) case displacements were 0.16 and 0.237 Å, respectively.

For the (100) surface of diamond both potential functions employed in this study predict that a (2×1) restructured dimer model is energetically more stable than the (1×1) unrestructured surface. This result is consistent with earlier calculations found in the literature [4-6]. Among three different (2×1) patterns considered here, the Brenner function gives the dimer model as the energetically most favorable structure. The Tersoff function, on the other hand, predicts the (MS+1) model to be the most stable configuration. So far, the dimer model has been proposed for the (2×1) reconstructed (100) surface of diamond by analogy with the Si(100) and Ge(100) surfaces. This model is very convincing and at the same time, it is well supported by theoretical calculations showing dimerization as an energetically favorable process. At the present time, however, there is not enough evidence indicating that the dimer model is the most favorable surface configuration leading to a (2×1) pattern. For that reason, perhaps, the choice of a

dimer model to explain the (2×1) LEED patterns may still need further substantiation. Despite many similarities, carbon in terms of structure, behaves somewhat differently than Si and Ge. For the bulk structure, for instance, the diamond phase is not the energetically most favorable one. More importantly, the (2×1) restructured (100) surface of diamond does not exhibit the higher order reconstruction patterns which have been observered for Si and Ge cases [3,9]. In order to fully resolve this issue, in addition to new experiments, more accurate *ab initio* calculations, perhaps for a number of different (2×1) patterns, are needed. Presently, we believe that the question "are there other (2×1) surface configurations with energies lower than the dimer model" remains unanswered for the (100) surface of diamond.

Results obtained in this investigation support the stability of the dimer model over the (1×1) unreconstructed (100) surface of diamond. In fact, calculations indicate that all three (2×1) patterns which were considered in this work are energetically more stable than the unreconstructed (1×1) face. In general, calculated energies and structural properties for the dimer model were found to be in agreement with values reported in the literature. While the Brenner function, in accordance with general belief, predicts the dimer model to be the energetically most stable structure, the Tersoff function produced one of the missing row models, (MR+1), as the energetically most favorable form. This last result, however, should be weighed with caution. It may be an indication of a flaw in the potential function or we need to reconsider the assumption that the dimer model is the lowest energy configuration for the (2×1) restructured surface.

References

[1] J. Tersoff, Phys. Rev. Lett., **61**, 2879 (1988).

[2] D. W. Brenner, Mater. Res. Soc. Symp. Proc., **141**, 59 (1989).

[3] A. V. Hamza, G. D. Kubiak and R. H. Stulen, Surf. Sci., **237**, 35 (1990).

[4] S. P. Mehandru and A. B. Anderson, Surf. Sci., **248**, 369 (1991).

[5] F. Bechstedt and D. Reichardt, Surf. Sci., **202**, 83 (1988).

[6] W. S. Verwoerd, Surf. Sci., **103**, 404 (1981).

[7] T. Halicioglu, Chem. Phys. Lett., **179**, 159 (1991).

[8] T. Halicioglu, Surf. Sci., (in press, 1991).

[9] D. Haneman, Rep. Prog. Phys., **50**, 1045 (1987).

Table 1. Structure and energy values for the (2×1) dimerized (100) surface of diamond (calculated by Tersoff and Brenner functions) compared with values from the literature. Relaxation energies, ΔE, are in eV per surface atom. The distance between two carbon atoms in a dimer is denoted by r_{dimer}. The change in the interlayer spacing between i and j layers is denoted by Δh_{ij} and δ_{ij} is the correponding per cent change with respect to the unrelaxed structure. All distances are in Å.

	Tersoff	Brenner	[4]	[5]	[6]
ΔE	−0.495	−1.134	−1.84 (−1.26)*	−0.41	−1.55
r_{dimer}	1.542	1.453	1.58 (1.40)*	1.54	1.434
Δh_{12}	−0.196	−0.266	−0.12 (−0.14)*		−0.24
δ_{12} (%)	−22.0	−30.6	−16.9 (−21.4)*		
Δh_{23}	0.012	0.124	0.03 (0.05)*		
δ_{23} (%)	1.34	14.2	6.7 (9.0)*		
Δh_{34}	0.	−0.01	−0.03 (−0.03)*		
δ_{34} (%)	0.	−1.0	−3.4 (−3.4)*		

* Spin paired results. See reference 4.

Table 2. Structure and energy values for (2×1) "Missing Row" models for the (100) surface of diamond calculated by Tersoff and Brenner functions. Descriptions of (MR) and (MR+1) models are given in the text. Relaxation energies, ΔE, are in eV per surface atom. The change in the interlayer spacing between i and j layers is denoted by Δh_{ij}; and δ_{ij} is the correponding per cent change with respect to the unrelaxed structure. The 0'th layer is for the (MR+1) case, it corresponds to the new layer formed by the displaced first layer atoms (see the text). All distances are in Å.

	Tersoff		Brenner	
	(MR)	(MR+1)	(MR)	(MR+1)
ΔE	−0.391	−0.820	−0.704	−0.955
Δh_{01}		−0.157		−0.252
δ_{01} (%)		−17.63		−29.05
Δh_{12}	−0.058	0.183	−0.098	0.234
δ_{12} (%)	−6.51	20.52	−11.29	26.91
Δh_{23}	−0.067	−0.092	−0.145	−0.156
δ_{23} (%)	−7.50	−10.31	−16.71	−17.90
Δh_{34}	0.009	0.010	0.024	0.019
δ_{34} (%)	1.04	1.22	2.75	2.23

Figure 1. A schematic top view for the (1×1) unreconstructed (100) surface of diamond. Positions of atoms located in the top three layers are shown. Large open circles represent top layer atoms. Small open circles indicate atoms in the second layer. Small solid circles are the third layer atoms.

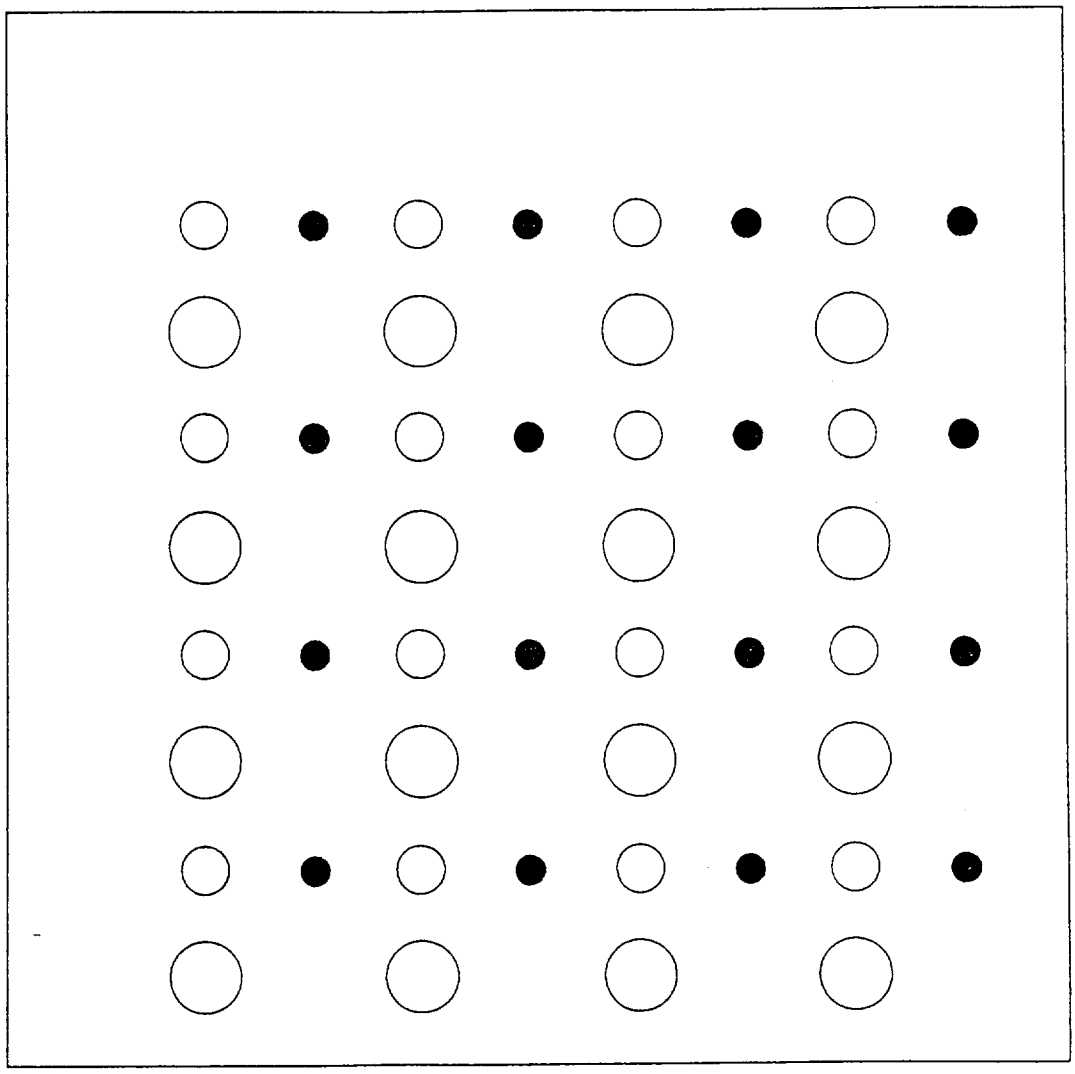

Figure 2. Top view of a (2×1) reconstructed missing row model (MR) for the (100) surface of diamond. This structure was generated by removing carbon atoms located in alternating rows. Positions of atoms located in the top three layers are shown. Large open circles represent top layer atoms. Small open circles indicate atomic positions in the second layer and small solid circles are the third layer atoms.

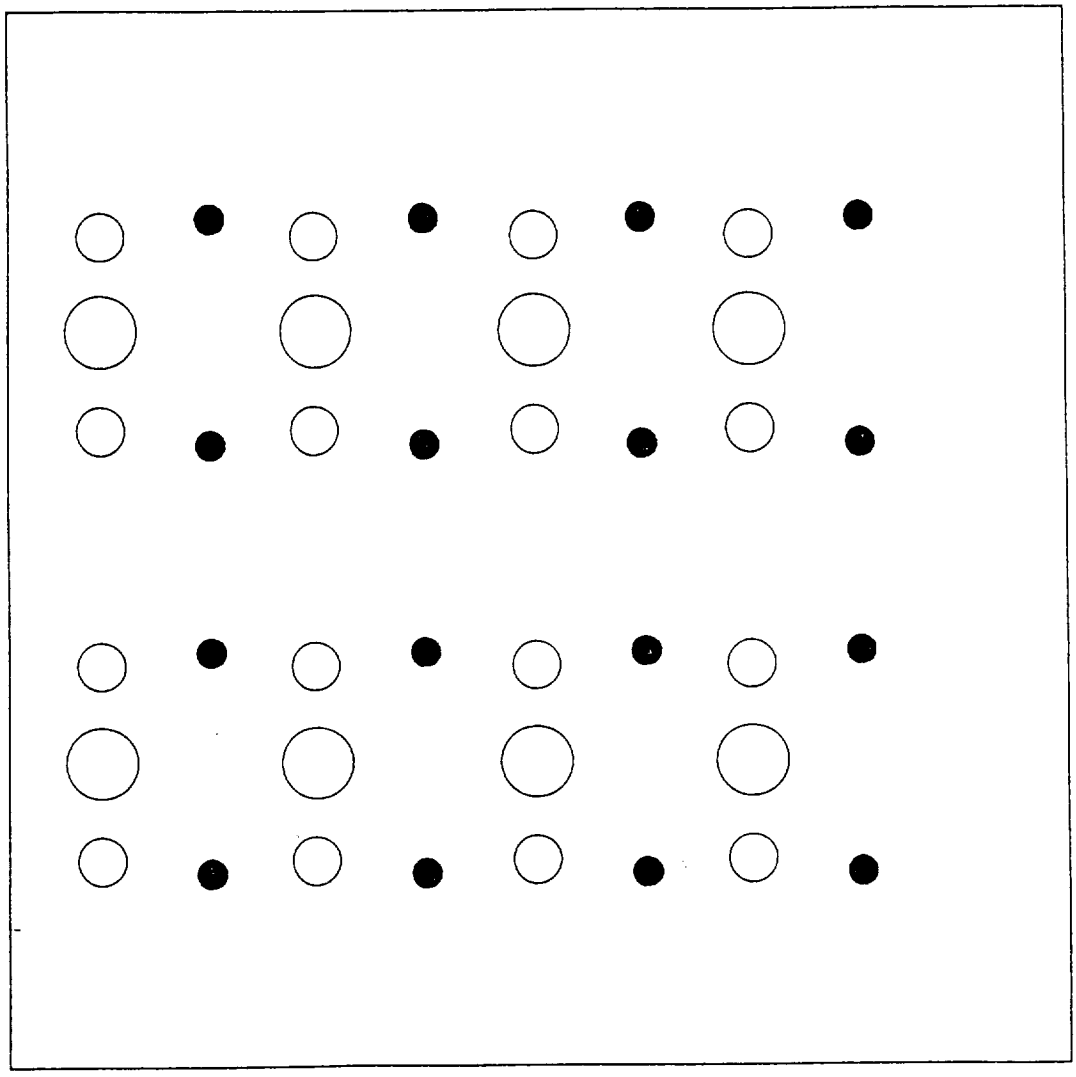

Figure 3. Top view of a (2×1) reconstructed missing row model (MR+1). In this structure, those atoms which were removed to generate the (MR) model, are introduced back into the system. They are placed on bridge sites of top layer atoms and shown by large open circles with a cross. These atoms constitute the 0'th layer as indicated in the text. Large open circles represent atoms in the first layer. Small open circles indicate atoms in the second layer. Small solid circles are the third layer atoms.

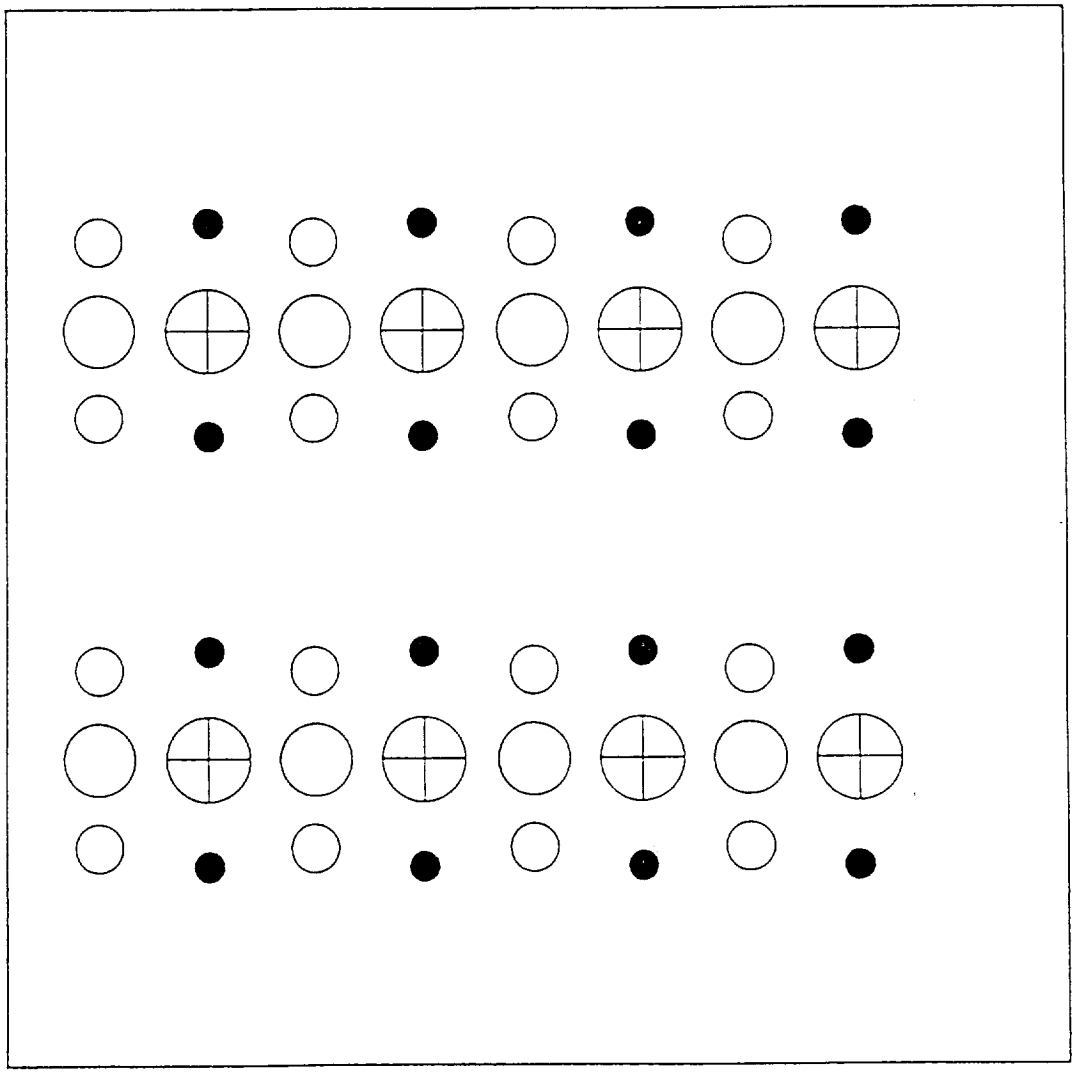

Figure 4. Top view of the (2×1) restructured dimer model for the (100) surface of diamond. Positions of atoms located in the top three layers are shown. Large open circles represent top layer atoms. Small open circles indicate atoms in the second layer. Small solid circles are the third layer atoms.

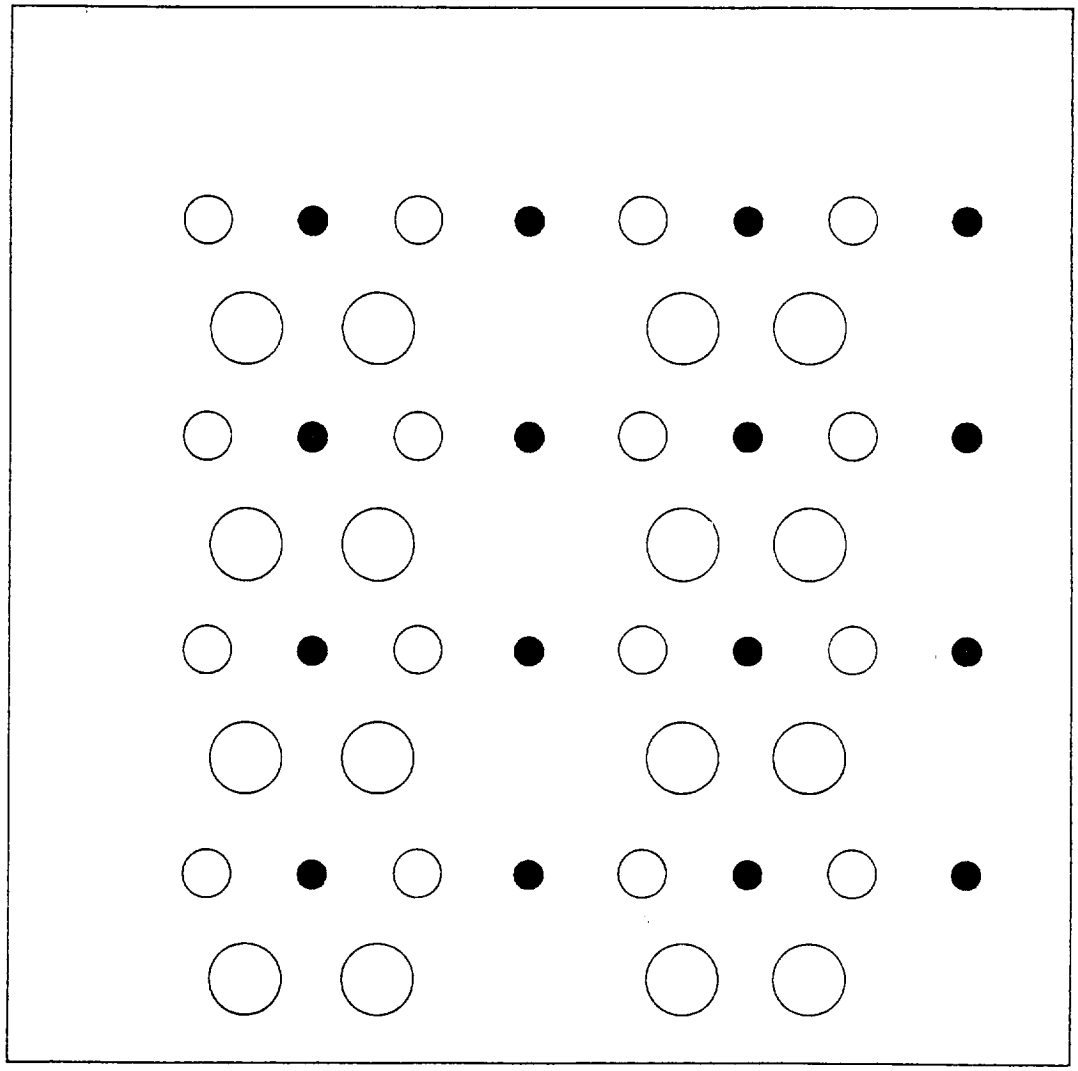

Appendix 3. Crack Propagation and Tensile Behavior for the Basal Plane of Graphite

The propagation of a surface crack was investigated at an atomistic level for a basal plane of graphite employing a computer simulation technique based on a molecular dynamics procedure. In addition to investigations of structural changes taking place during the crack propagation, in this study, the distribution of atomic stresses at the crack tip was also analyzed. Simulation calculations were carried out considering a potential function which has been derived recently by Tersoff [1] to represent energy- and structure-related properties of carbon systems. The Tersoff function, to date, has been used quite successfully in many studies. In addition to its ability to reproduce properties of a graphitic plane, this function can also predict many surface and bulk properties of the diamond phase. The total potential energy of a system of N particles in the Tersoff potential is expressed as a sum over atomic sites of the form:

$$\Phi = \sum_{i}^{N} E_i \tag{1}$$

with

$$E_i = \frac{1}{2} \sum_{j(\neq i)}^{N} f_c(r_{ij})[V_R(r_{ij}) - b_{ij} V_A(r_{ij})] \tag{2}$$

where, r_{ij} denotes the internuclear distance between particles i and j, and $f_c(r_{ij})$ represents the cut-off function which is given by:

$$f_c(r_{ij}) = \begin{cases} 1, & \text{if } r_{ij} < R - D; \\ \frac{1}{2} - \frac{1}{2} sin[\frac{\pi}{2}(r_{ij} - D)/D], & \text{if } R - D < r_{ij} < R + D; \\ 0, & \text{if } r_{ij} > R + D. \end{cases} \tag{3}$$

The three-body part of the interactions is introduced via the function b_{ij}, while V_R and V_B represent repulsive and attractive parts, respectively. These functions were defined by Tersoff as:

$$V_R(r_{ij}) = A \cdot exp(-\lambda_1 r_{ij})$$

$$V_A(r_{ij}) = B \cdot exp(-\lambda_2 r_{ij})$$

$$b_{ij} = (1 + \beta^n \xi_{ij}^n)^{-1/2n}$$

$$\xi_{ij} = \sum_{k(\neq i,j)}^{N} f_c(r_{ik}) \cdot g(\theta_{ijk}) \cdot exp[\lambda_3^3 (r_{ij} - r_{ik})^3]$$

$$g(\theta_{ijk}) = 1 + c^2/d^2 - c^2/[d^2 + (h - cos\theta_{ijk})^2]$$

For carbon the Tersoff parameters are given as: $A = 1393.6(eV)$, $B = 346.74(eV)$, $\lambda_1 = 3.4879(\mathring{A})$, $\lambda_2 = 2.2119(\mathring{A})$, $\beta = 1.5724 \times 10^{-7}$, $n = 0.72751$, $c = 38049.$, $d = 4.3484$, $h = -0.57058$, $R = 1.95(\mathring{A})$ and $D = 0.15(\mathring{A})$.

Calculations were carried out considering a constant temperature molecular dynamics technique based on the Verlet algorithm [2]. Throughout this study a time step of $5. \times 10^{-16}$ sec. and a reduced temperature of 0.25 were employed. Stresses for each atom in the system were evaluated as:

$$\sigma_{\alpha\beta} = \frac{1}{v}(\frac{\partial E_i}{\partial \eta_{\alpha\beta}})$$

where, $\sigma_{\alpha\beta}$ denotes the atomic stress for the Cartesian components α and β, and $\eta_{\alpha\beta}$ represents the corresponding Lagrangian strain parameter [3]. The volume and the energy for the i'th atom are denoted by v and E_i, respectively. The model used in this study representing the basal plane of graphite contained 840 (30×28) atoms arranged in a rectangular two-dimensional array. First, a perfect lattice in a 2D honeycomb structure was brought to a static equilbrium. This system displays an almost elastic behavior and it resists any plastic deformation up to relatively high strain values. A crack was generated in this 2D system by removing 9 atoms from the surface region. A portion of this system with the crack is shown schematically in Figure 1. Then, a uniaxial load along the x direction was imposed on the system (which now bears a surface crack) in a stepwise fashion by progressively increasing the total length of the system in small increments. At any given time the actual elongation, e, is defined as:

$$e = \frac{l - l_o}{l_o}$$

where, l_o and l denote the lengths of the system in x direction at the initial stage (i.e., at time $t = 0$) and at a time t during the loading process. A periodic boundary condition was applied also in the x direction to provide continuity. In the perpendicular y direction, on the other hand, two exposed surfaces, one bearing the initial crack, were left intact.

After the initial 1000 equilibration time steps, the system with a surface crack was elongated with small increments ($\Delta e = 0.005$). Following each incremental elongation, the system was permitted to equilibrate for 50 time steps under the molecular dynamics code. In this second stage, the incremental loading and equilibration process was repeated 30 times corresponding to a total elongation of $e = 0.161$. During the final stage, no elongation was performed, but the system was simply permitted to relax for an extented period of time to observe the approach of the system to equilibrium. In Figure 2 a plot is presented displaying the elongation and the variation of the total energy of the system as a function of time steps. Except the very first few steps, the energy remains virtually constant during the first equilibration period. In the second stage, as expected, the energy increases progressively with the loading. Perhaps one may assume that at least in the beginning part of the second stage the system behaves elastically. As the existing crack propagates the stress is released and, as expected, the average energy of the system decreases. Figure 3 displays the variation of the average stress during the loading and equilibration stages. The phonon field generated in the lattice and its approach to equilibrium is visible in the final equilibration stage. These fluctuations in the stress value represent thermal effects [4]. Figures 4a through 4k display configurations of the system at various stages during the final relaxation period. As shown in these schematic drawings, the surface crack starts propagating after the 2500 th step. The solid circles in these figures represent 15 atoms with the largest stress values. In all cases, during the propagation period the tip of the crack exhibited itself as the high stress zone. This outcome is in general argeement with continuum studies. The crack propagates virtually perpedicular to the load direction. In this

study, no dislocation formation was observed in front of the crack tip. In order to investigate the size dependence of these results, calculations were repeated using a larger model containing 1680 (60×28) atoms. This larger system was found to produce results basically identical to those obtained by the smaller model. The time dependence of the propagation and the distribution of the high stress atoms as well as the crack tip geometry were all found to be very similar.

In this case, only a very highly strained (e=0.161) system was taken into consideration. Despite the fact that present calculations correctly predict some of the contiuum results (such as the crack tip being the high stress zone), further calculations with less strained systems are needed for a more complete analysis. Present calculations constitute the very first part of a general study on the simulation of crack propagation processes for covalently bonded systems. A proper representation of atomic interactions in covalently bonded systems requires consideration of potential functions based on many-body interactions (like the Tersoff function employed here). One of the important features of the many-body interactions is to provide energetically stable configurations for open systems like the graphitic basal plane. In a crack propagation process, on the other hand, the role played by many-body forces constitutes a somewhat more complex academic problem; therefore, it will be addressed separately. When these present results are compared with earlier calculations, the very short nature of the Tersoff function must be kept in mind. Furthermore, the ability of this function to simulate materials properties (in particular, those based on long range interactions) must be thoroughly analyzed. Another important point, in this respect, is related to dislocations. The absence of dislocations in this study may come from the brittle character of the model system considered here, or, more convincingly perhaps, it is due to the short range nature of the potential function employed.

References

[1] J. Tersoff, Phys. Rev. Lett., **61**, 2879 (1988).

[2] D. Fincham, Comp. Phys. Comm., **21**, 247 (1980).

[3] D. C. Wallace, *"Thermodynamics of Crystals"*, (John Wiley, 1972).

[4] T. Halicioglu and D. M. Cooper, Mater. Sci. Eng., **79**, 157 (1986).

Figure 1. A schematic representation for the initial configuration of the system with a surface crack.

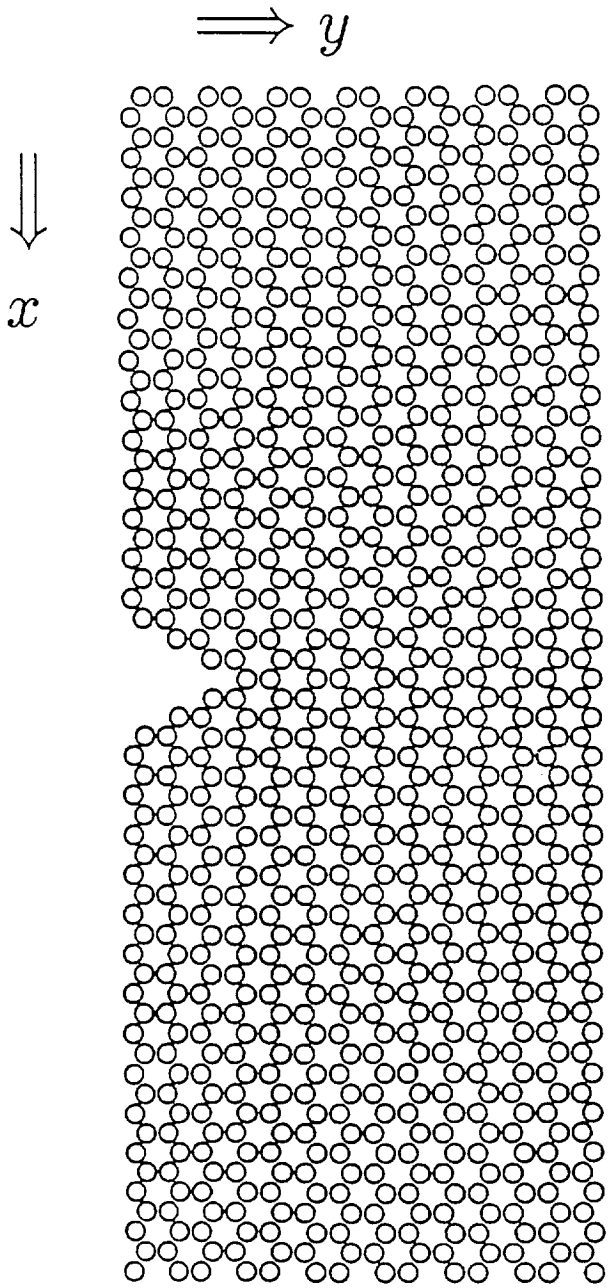

Figure 2. Variations in the total energy and in the elongation as a function of time steps.

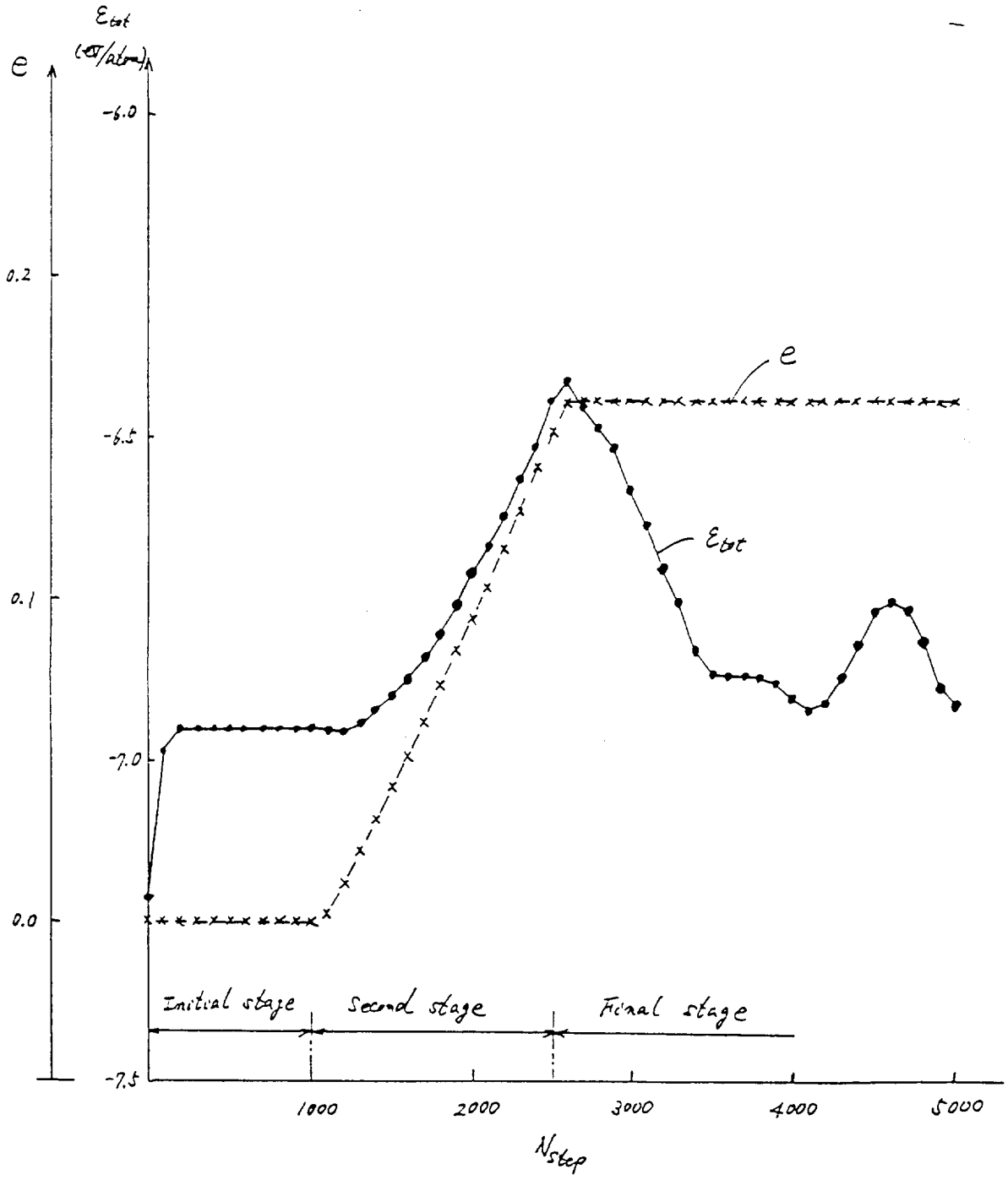

Figure 3. Average stress values are shown versus time steps.

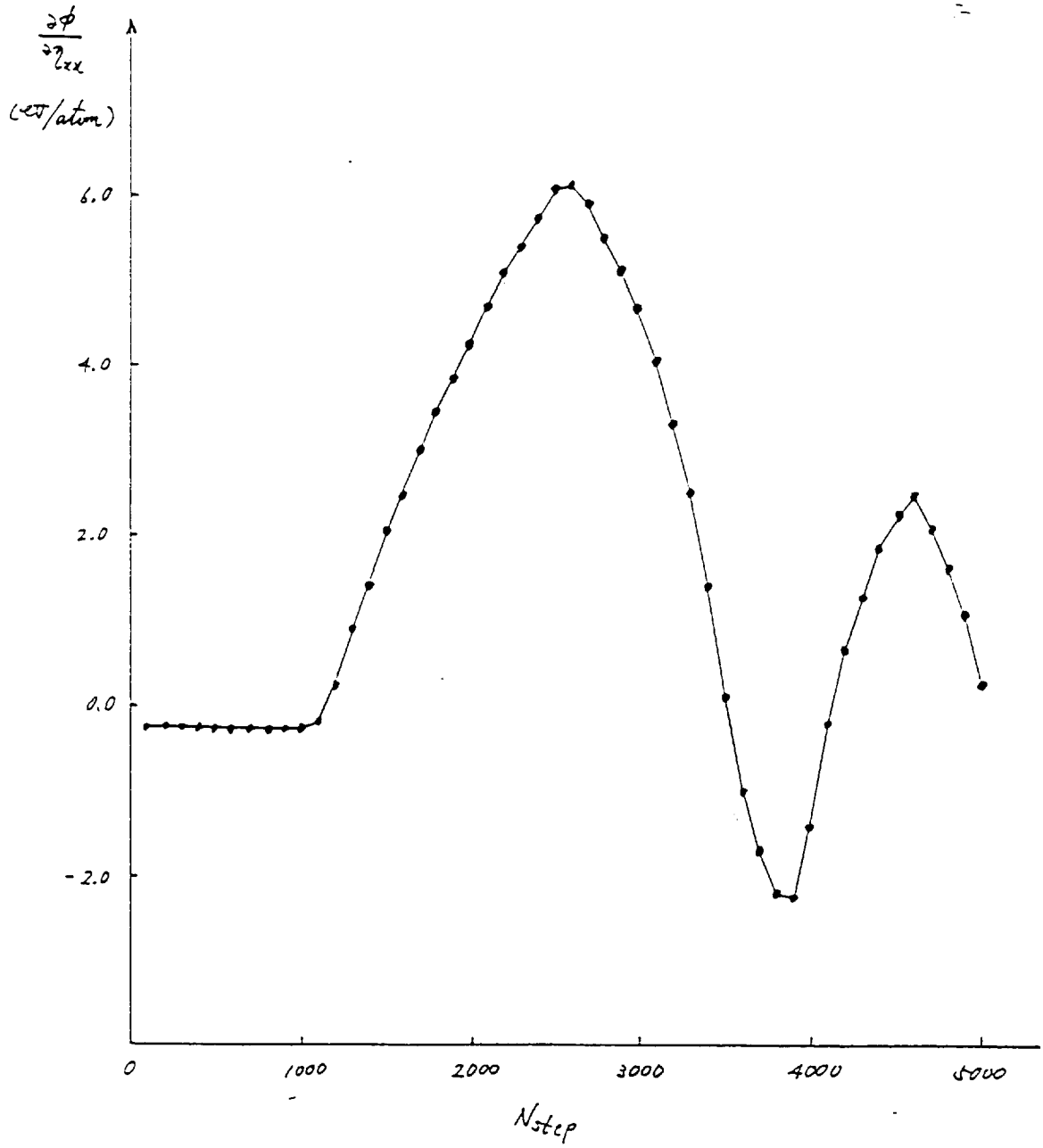

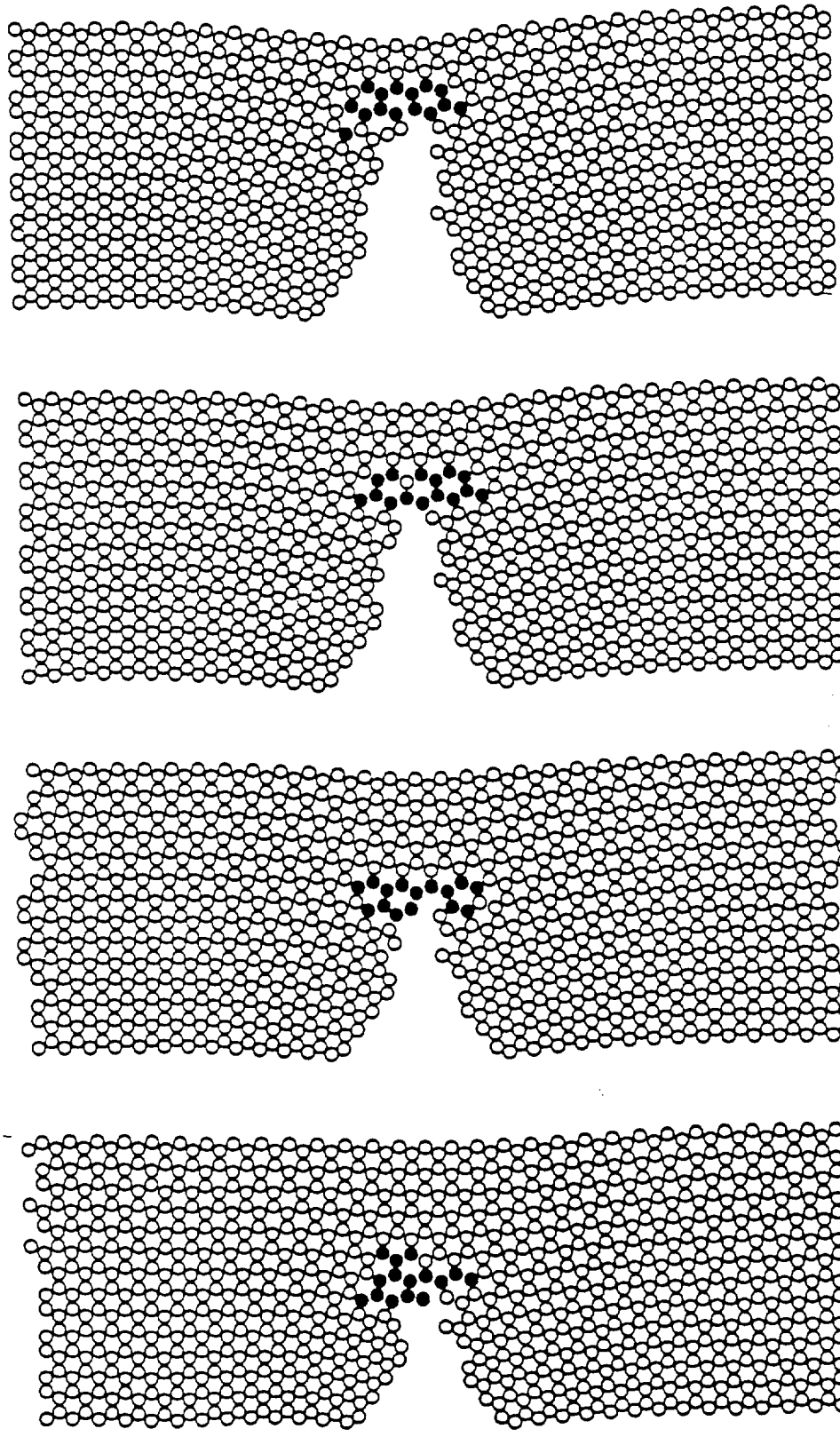
3100
(h)
3000
(g)
2900
(f)
2800
(e)

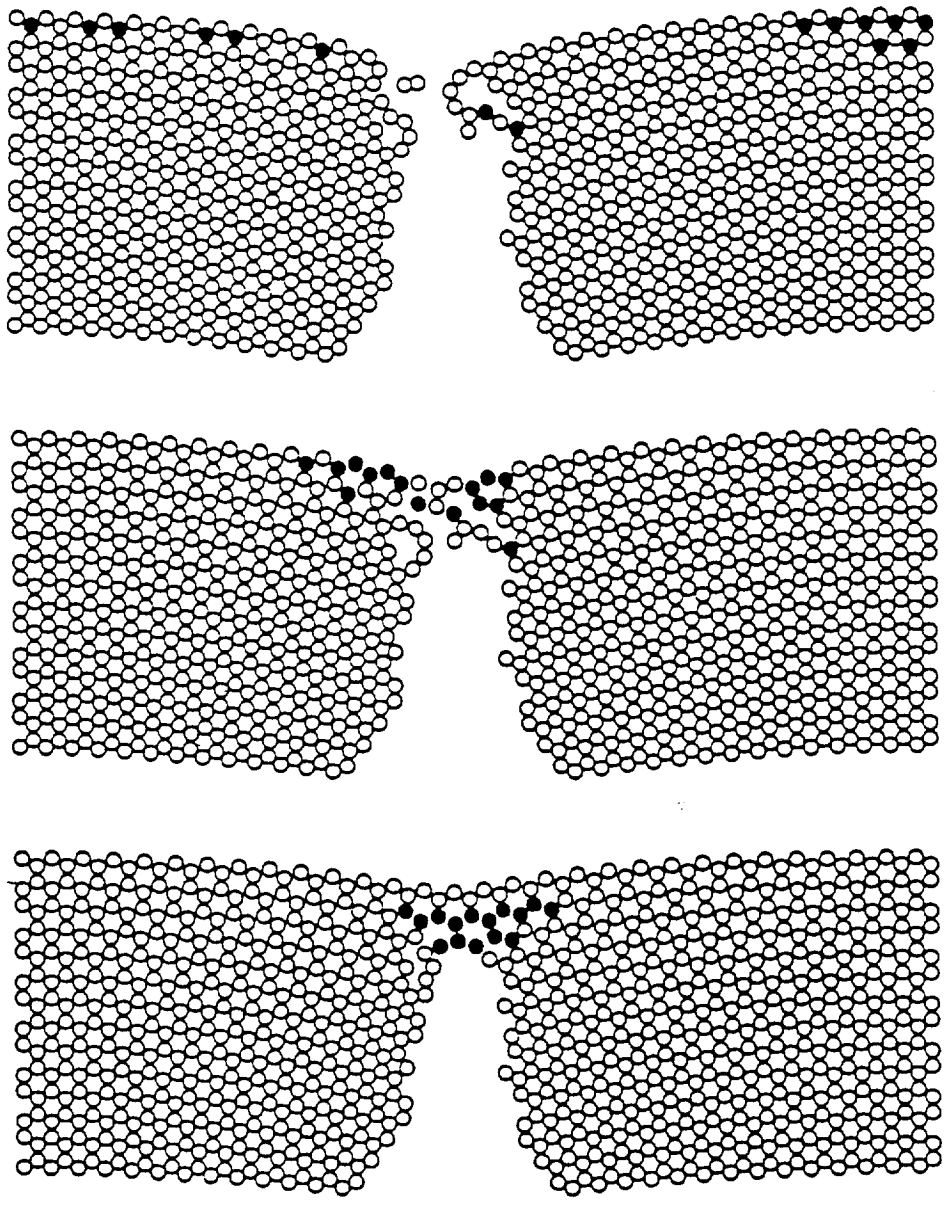
3400
(k)
3300
(j)
3200
(i)